Delayed differential equation based study of sub-terahertz emission in multi-section quantum dot ring lasers

Delayed differential equation based study of sub-terahertz emission in multi-section quantum dot ring lasers

Emanuele Groppo[a], Lorenzo Tunesi[a], and Paolo Bardella[a]

[a]Department of Electronics and Telecommunications, Politecnico di Torino, Torino, Italy.

ABSTRACT

We present a study of the generation of subterahertz pulses in multi-section quantum dot (QD) ring lasers based on an improved version of the well-established delayed differential equation model, and taking into account an arbitrary number of gain and absorber sections. Results of the analysis of an 8-section ring laser emitting at 1.3 µm are presented. The proposed approach provides a significant insight for the understanding of the onset of the harmonic mode-locking in this family of devices and shows to be an effective tool for the optimization of the real devices in terms of pulses quality and generated RF intensity.

Keywords: Quantum Dot, Sub-terahertz emission, delayed differential equation

1. INTRODUCTION

Compact on-chip RF signal sources are key components for the development of applications beyond 5G[1], requiring high-frequency bandwidth. The sub-terahertz range (between 90 GHz and 300 GHz) is particularly attractive as new wireless transmission window, as it provides a set of significant advantages compared with other wireless communication links[2]. With respect to microwave communications, sub-terahertz ones intrinsically allow the transmission of ultra-broadband data, they are less affected by free-space diffraction phenomena, and less sensitive to bad weather conditions and with respect to higher frequency bands (e.g. infra-red bands)[3].

Although femtosecond pulse sources[4] and photoconductive switches[5] are two solutions typically used for broadband THz generation in commercial systems, they present serious drawbacks in terms of cost, power consumption and large footprint.

An interesting alternative solution is represented by Mode-locking (ML) and gain switching lasers, two techniques that can be exploited for ultra-short pulse generation.[6–11] The fundamental repetition frequency f_{R} in a passive ML semiconductor laser is inversely proportional to the cavity length L of the device, which should therefore be rather short to achieve high emission frequencies. This technological limit can be overcome by moving to harmonic ML solutions, in which two or more pulses are circulating in the laser cavity, providing an overall repetition rate which is an integer multiple of the fundamental one.[12,13]

Here, we propose a model for the study of the dynamical behavior of multi-section unidirectional ring lasers operating the sub-THz region, based on the delayed differential equation (DDE) model.[14,15] The manuscript is organized as follows: in Section II we present the fundamentals of the DDE model, while in Section III we introduce a reference QD ring laser configuration with four gain regions and four inversely biased regions and summarize the corresponding DDE simulation results. Finally, in Section IV we draw our conclusions.

2. DELAYED DIFFERENTIAL EQUATION MODEL

We extended the Multi-Section Delayed Differential Equation (MS-DDE) model[14] to study the temporal evolution of the multisection laser. The model proposed by Rossetti et al.[14] can be used to study the emission from both the ground state (GS) and the first excited state (ES)[9]: this possibility has been conserved in the updated version. The electric field at the selected output facet for Ground State (GS) and first Excited State (ES1) emission reads

$$\frac{\mathrm{d}E_i(\tau)}{\mathrm{d}t} = -\gamma E_i(\tau) + \gamma R_i(\tau - T_{\mathrm{R}})\, E_i(\tau - T_{\mathrm{R}}) \tag{1}$$

Send correspondence to Paolo Bardella. E-mail: paolo.bardella@polito.it

where the index $i = \mathrm{GS}, \mathrm{ES1}$ represents the energy level considered and the term γ describes the gain broadening of the QD ensemble. The cold cavity round-trip time is calculated as

$$T_{\mathrm{R}} = L_{\mathrm{ring}}/v_{\mathrm{g}} \tag{2}$$

with $L_{\mathrm{ring}} = \sum_{k=1}^{F} L_k$ the total cavity length (given by the sum of the F sections lengths) and $v_{\mathrm{g}} = c/n_{\mathrm{r}}$ the group velocity. Finally, R_i is the round-trip gain experienced by the pulse during the propagation in the various device sections, can be computed as

$$R_i(\tau) = \prod_{k=1}^{F} B_{i,k}(\tau)\, M_k \tag{3}$$

with M_k non-saturable losses localized between the k^{th} and the $(k+1)^{\mathrm{th}}$ sections, including intrinsic waveguide losses experienced by the field when propagating across the k^{th} section and output losses localized at the coupling interface:

$$M_k = \sqrt{K_k}\mathrm{e}^{\left(-\frac{\alpha_{\mathrm{i}}}{2} L_k\right)}. \tag{4}$$

The term $B_{i,k}(\tau)$ instead represents the amplification (or attenuation) and the phase change experienced by the field when propagating across the k^{th} section:

$$B_{\mathrm{GS},k}(\tau) = \mathrm{e}^{\left(\Gamma_{xy}\overline{g}_{\mathrm{GS},k}(\tau)L_k\right)}\mathrm{e}^{\left(\mathrm{j}\,\beta\Gamma_{xy}\overline{g}_{\mathrm{ES1},k}(\tau)L_k\right)} \tag{5}$$

$$B_{\mathrm{ES1},k}(\tau) = \mathrm{e}^{\left(\Gamma_{xy}\overline{g}_{\mathrm{ES1},k}(\tau)L_k\right)}\mathrm{e}^{\left(-\mathrm{j}\,\beta\Gamma_{xy}\overline{g}_{\mathrm{GS},k}(\tau)L_k\right)}. \tag{6}$$

with β coefficient indicating the frequency separation between GS and ES1:

$$\beta = \gamma\frac{\omega_{\mathrm{ES1}} - \omega_{\mathrm{GS}}}{\gamma^2 + \left(\omega_{\mathrm{ES1}} - \omega_{\mathrm{GS}}\right)^2} \tag{7}$$

In Eqs. (5) and (6), the gain/absorption introduced by the QD at the GS or ES1 wavelengths in the k^{th} section is calculated as

$$\overline{g}_{i,k}(\tau) = g_{0,i}\left(2\overline{\rho}_{i,k}(\tau) - 1\right) \tag{8}$$

where $\overline{\rho}_{i,k}(\tau)$ represents the occupation probability in the i^{th} QD state averaged over the k^{th} section and whose temporal dynamics in each section of the ring cavity is computed via a system of rate equations:

$$\frac{\mathrm{d}\overline{\rho}_{i,k}(\tau)}{\mathrm{d}\tau} = \overline{R}^{\mathrm{in}}_{i,k}(\tau) - \overline{R}^{\mathrm{out}}_{i,k}(\tau) - \overline{R}^{\mathrm{stim}}_{i,k}(\tau). \tag{9}$$

with $\overline{R}^{\mathrm{in}}_{i,k}(\tau)$ injection rate, $\overline{R}^{\mathrm{out}}_{i,k}(\tau)$ escape rates and $\overline{R}^{\mathrm{stim}}_{i,k}(\tau)$ recombination rate by stimulated emission.[16] The description of the carrier dynamics in the QD material is completed by rate equations describing the evolution of the number of carriers in the 2D wetting layer and in the 3D Separate Confinement Heterostructure (SCH).[11,16] Figure 1(a) shows the energy levels of the analyzed structure at thermal equilibrium, with the set of time constants associated to the various inter-band mechanisms. In the saturable absorber (SA), in the presence of an applied reverse voltage, the electric field in the growth direction x introduces additional phenomena, such as carrier tunneling from QD and WL energy levels to the SCH, as shown in Figure 1(b).[17]

Finally, the output power after a full round trip (that is, at the end of the F^{th} section) is evaluated as

$$P_i^{\mathrm{out}}(\tau) = \frac{1 - K_F}{K_F}\left|E_i(\tau)\right|^2. \tag{10}$$

3. SIMULATION RESULTS

The described MS-DDE model allows for the description of both edge-emitting and ring-shaped QD lasers, whose structure is sliced into F sections in which the presented equations are solved. The results obtained for the ring laser structure schematically depicted in Figure 2 are discussed below. The device emits at a wavelength of 1.3 µm corresponding to the GS energy transition. The main physical parameters are summarized in Table 1.

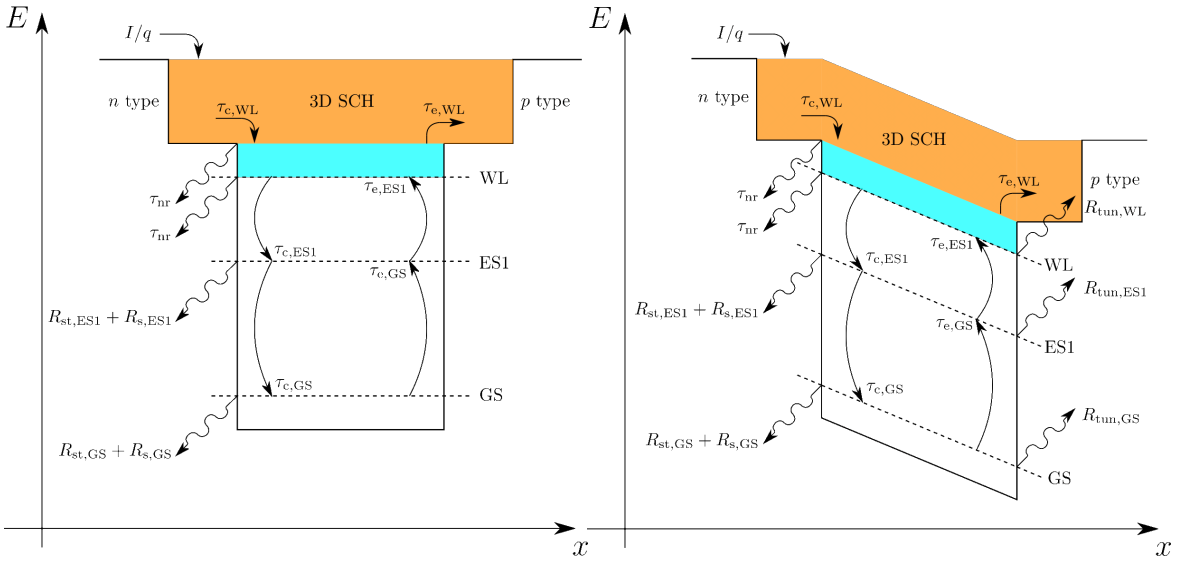

Figure 1: Energy levels in a current-driven section (a) and in a reversely biased section (b).

The cavity is made up of four interleaved active and absorbing sections. The total length of the cavity is $L_{\text{ring}} = 4.38\,\text{mm}$. Each SA section has a length equal to 5.8% of the total ring length. The corresponding fundamental repetition rate is approximately $f_{\text{R}} = 18.75\,\text{GHz}$. Due to the specific configuration of the cavity, we expect to observe a region with ML at 75 GHz, i.e. four times f_{R}.

The device behavior has been analyzed in the active region current vs. reverse bias voltage plane, checking for each point if a periodic behavior of the generated power is observed, and then extracting the repetition frequency from the RF spectrum. The stability of the pulses in terms of leading- and trailing-edge instabilities is also investigated.

The main results of this work are reported in Figure 3. The colors allow an easy evaluation of the achieved pulsation frequency with respect to the fundamental one, depending on the chosen bias values. Superimposed on this map, the instability regions are highlighted by oblique black lines, determined according to Haus criterion.[18] In particular, the net gain in the active material must become negative immediately after the ML pulse has passed, otherwise spontaneous emission noise may be amplified by a net gain window following the pulse trailing edge, leading to instability. For the device considered, the target region is the green one, corresponding to a ML at $f = 4 \times f_{\text{R}} = 75\,\text{GHz}$. However, we also observe a region of stable ML at the fundamental frequency f_{R}; unstable operation at f_{R}, $2f_{\text{R}}$, and $8f_{\text{R}}$ is also reported.

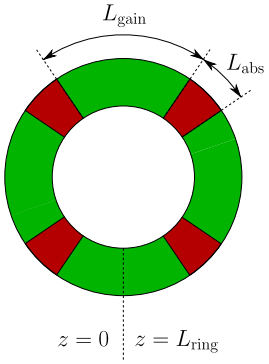

Figure 2: Reference ring structure.

Symbol	Description	Value
d	Ridge waveguide width	6 µm
α_{i}	Intrinsic waveguide losses	1.5 cm^{-1}
Γ_{xy}	Confinement factor	0.075
h_{SCH}	SCH height	180 nm
h_{QW}	QW height	7 nm
h_{QD}	QD height	5 nm
N_{l}	QD layers	12
N_{D}	QD surface density	2.85×10^{10} cm^2
$\hbar\gamma$	FWHM inhomogeneous gain broadening	34 meV
E_{GS}	GS energy level	0.9904 eV
E_{ES1}	ES1 energy level	1.0597 eV
$\tau_{\mathrm{c,GS}}$	GS capture time	0.3 ps
$\tau_{\mathrm{c,ES1}}$	ES1 capture time	0.3 ps
$g_{0,\mathrm{ES1}}$	ES1 maximum gain	330 cm^{-1}
$g_{0,\mathrm{GS}}$	GS maximum gain	190 cm^{-1}
V_{bi}	Built-in potential	0.8 V

Table 1: Main physical parameters used in the simulation.

In the design phase of the whole system, the bias values have to be chosen accordingly in order to obtain a stable pulse train. An exemplary comparison between the stable and unstable points of the map is reported here, considering points A ($I = 260\,\mathrm{mA}$, $V = -5\,\mathrm{V}$) and B ($I = 260\,\mathrm{mA}$, $V = -6\,\mathrm{V}$) identified in the map.

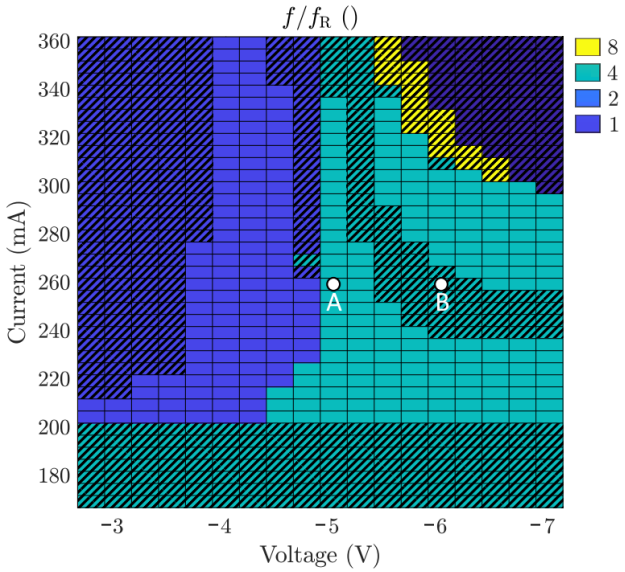

Figure 3: Repetition rate w.r.t. f_{R}. Non-stable regions are indicated by oblique lines. Bias points A and B are discussed in the text.

Bias point A is characterized by the required frequency, equal to $f = 4 \times f_{\mathrm{R}} = 75\,\mathrm{GHz}$. Consequently, four pulses can be identified within a round-trip period $T_{\mathrm{R}} = 53.5\,\mathrm{ps}$, as it is shown in the graph of Figure 4(a). This type of oscillation is stable according to the above-mentioned criteria. The pulse width, computed from the autocorrelation of the pulses assuming a Gaussian shape, is 3.84 ps.

On the contrary, the bias point B cannot be considered acceptable for the operation of the device. Despite showing the correct output frequency, the pulses are characterized by a strong trailing edge instability, as shown in Figure 4(b).

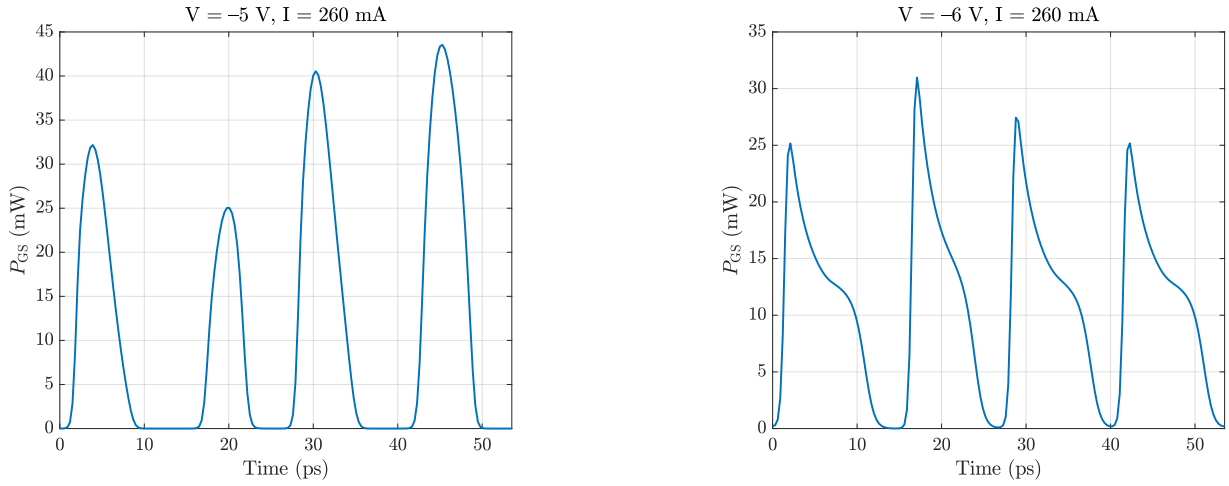

(a) (b)

Figure 4: Temporal evolution of the generated power at GS wavelength for (a) bias point A and (b) bias point B in Fig. 3.

4. CONCLUSIONS

We proposed a generalization of the MS-DDE model, introducing the possibility to simulate lasers constituted of several active and reversely biased sections. Within this type of structure, ML regimes can take place at multiples of the fundamental cavity repetition frequency, and the generalization of the model allows the study of devices where the emission sub-THz pulses occurs. The simulations carried out with MS-DDE are computationally efficient with respect to other approaches such as the Time-domain Travelling-Wave method,[16] thus providing a valid solution to the generation of maps in the current-voltage plane. As an example, we discussed the behavior of a ring QD laser with 4 active and 4 reversely biased regions and we reported stable pulsed operation conditions at 4 times the fundamental repetition rate.

REFERENCES

[1] Song, H.-J. and Nagatsuma, T., "Present and future of terahertz communications," *IEEE transactions on terahertz science and technology* **1**(1), 256–263 (2011).

[2] Federici, J. and Moeller, L., "Review of terahertz and subterahertz wireless communications," *Journal of Applied Physics* **107**(11), 6 (2010).

[3] Piesiewicz, R., Jansen, C., Mittleman, D., Kleine-Ostmann, T., Koch, M., and Kurner, T., "Scattering analysis for the modeling of thz communication systems," *IEEE Transactions on Antennas and Propagation* **55**(11), 3002–3009 (2007).

[4] Brown, C. T., Cataluna, M. A., Lagatsky, A., Rafailov, E. U., Agate, M., Leburn, C., and Sibbett, W., "Compact laser-diode-based femtosecond sources," *New Journal of Physics* **6**(1), 175 (2004).

[5] Panagamuwa, C. J., Chauraya, A., and Vardaxoglou, J., "Frequency and beam reconfigurable antenna using photoconducting switches," *IEEE Transactions on Antennas and Propagation* **54**(2), 449–454 (2006).

[6] Keller, U., "Recent developments in compact ultrafast lasers," *Nature* **424**(6950), 831–838 (2003).

[7] Wang, F., Pistore, V., Riesch, M., Nong, H., Vigneron, P.-B., Colombelli, R., Parillaud, O., Mangeney, J., Tignon, J., Jirauschek, C., et al., "Ultrafast response of harmonic modelocked THz lasers," *Light: Science & Applications* **9**(1), 1–8 (2020).

[8] Ryvkin, B., Avrutin, E. A., and Kostamovaara, J. T., "Asymmetric-waveguide laser diode for high-power optical pulse generation by gain switching," *Journal of Lightwave Technology* **27**(12), 2125–2131 (2009).

[9] Xu, T., Rossetti, M., Bardella, P., and Montrosset, I., "Simulation and analysis of dynamic regimes involving ground and excited state transitions in quantum dot passively mode-locked lasers," *IEEE Journal of Quantum Electronics* **48**(9), 1193–1202 (2012).

[10] Ding, Y., Alhazime, A., Nikitichev, D., Fedorova, K., Ruiz, M., Tran, M., Robert, Y., Kapsalis, A., Simos, H., Mesaritakis, C., Xu, T., Bardella, P., Rossetti, M., Krestnikov, I., Livshits, D., Montrosset, I., Syvridis, D., Cataluna, M. A., Krakowski, M., and Rafailov, E., "Tunable master-oscillator power-amplifier based on chirped quantum-dot structures," *IEEE Photonics Technology Letters* **24**(20), 1841–1844 (2012).

[11] Weber, C., Columbo, L. L., Gioannini, M., Breuer, S., and Bardella, P., "Threshold behavior of optical frequency comb self-generation in an inas/ingaas quantum dot laser," *Opt. Lett.* **44**, 3478–3481 (Jul 2019).

[12] Avrutin, E., Marsh, J., and Portnoi, E., "Monolithic and multi-gigahertz mode-locked semiconductor lasers: constructions, experiments, models and applications," *IEE Proceedings-Optoelectronics* **147**(4), 251–278 (2000).

[13] Hohimer, J. and Vawter, G., "Passive mode locking of monolithic semiconductor ring lasers at 86 ghz," *Applied physics letters* **63**(12), 1598–1600 (1993).

[14] Rossetti, M., Bardella, P., and Montrosset, I., "Modeling passive mode-locking in quantum dot lasers: A comparison between a finite-difference traveling-wave model and a delayed differential equation approach," *IEEE Journal of Quantum Electronics* **47**(5), 569–576 (2011).

[15] Rossetti, M., Xu, T., Bardella, P., and Montrosset, I., "Impact of gain saturation on passive mode locking regimes in quantum dot lasers with straight and tapered waveguides," *IEEE Journal of Quantum Electronics* **47**(11), 1404–1413 (2011).

[16] Rossetti, M., Bardella, P., and Montrosset, I., "Time-domain travelling-wave model for quantum dot passively mode-locked lasers," *IEEE Journal of Quantum Electronics* **47**(2), 139–150 (2011).

[17] Malins, D. B., Gomez-Iglesias, A., White, S. J., Sibbett, W., Miller, A., and Rafailov, E. U., "Ultrafast electroabsorption dynamics in an InAs quantum dot saturable absorber at 1.3 μm," *Applied Physics Letters* **89**(17), 171111 (2006).

[18] Haus, H., "Theory of mode locking with a slow saturable absorber," *IEEE Journal of Quantum Electronics* **11**(9), 736–746 (1975).